Giant spin gap and magnon localization in the disordered Heisenberg antiferromagnet $Sr_2Ir_{1-x}Ru_xO_4$

Yue Cao,[1,*] X. Liu,[2,3,†] Wenhu Xu,[1,‡] Wei-Guo Yin,[1] D. Meyers,[1] Jungho Kim,[4] Diego Casa,[4] M. H. Upton,[4] Thomas Gog,[4] Tom Berlijn,[5] Gonzalo Alvarez,[5] Shujuan Yuan,[6] Jasminka Terzic,[6] J. M. Tranquada,[1] John P. Hill,[7] Gang Cao,[6] Robert M. Konik,[1] and M. P. M. Dean[1,§]

[1]*Condensed Matter Physics and Material Science Department, Brookhaven National Laboratory, Upton, New York 11973, USA*
[2]*Beijing National Laboratory for Condensed Matter Physics and Institute of Physics, Chinese Academy of Sciences, Beijing 100190, China*
[3]*Collaborative Innovation Center of Quantum Matter, Beijing, China*
[4]*Advanced Photon Source, Argonne National Laboratory, Lemont, Illinois 60439, USA*
[5]*Computer Science and Mathematics Division and Center for Nanophase Materials Sciences, Oak Ridge National Laboratory, Oak Ridge, Tennessee 37831, USA*
[6]*Department of Physics, University of Colorado at Boulder, Boulder, Colorado 80309, USA*
[7]*National Synchrotron Light Source II (NSLS-II), Brookhaven National Laboratory, Upton, New York 11973, USA*
(Received 10 August 2016; revised manuscript received 25 January 2017; published 6 March 2017)

We study the evolution of magnetic excitations in the disordered two-dimensional antiferromagnet $Sr_2Ir_{1-x}Ru_xO_4$. The maximum energy of the magnetic excitation remains robust up to $x = 0.77$, with a gap opening at low dopings and increasing to over 150 meV at $x = 0.77$. At these higher Ru concentrations, the dispersive magnetic excitations in Sr_2IrO_4 are rendered essentially momentum independent. Up to a Ru concentration of $x = 0.77$, both experiments and first-principles calculations show the Ir $J_{\text{eff}} = 1/2$ state remains intact. The magnetic gap arises from the local interaction anisotropy in the proximity of the Ru disorder. Under the coherent potential approximation, we reproduce the experimental magnetic excitations using the disordered Heisenberg antiferromagnetic model with suppressed next-nearest-neighbor ferromagnetic coupling.

Many of the most interesting phases in condensed matter are accessed by chemically substituting (that is, doping) well-ordered crystalline materials. A particularly notable example is high temperature superconductivity in the cuprates which arises when the quasi-two-dimensional (2D) antiferromagnetic Mott insulating phase in the parent compounds is suppressed. For this reason, understanding the behavior of antiferromagnets in different doping regimes has become a quintessential problem in quantum magnetism [1–5]. The majority of experimental work [6–9] has focused on out-of-plane chemical substitutions that simultaneously introduce mobile carriers and weak disorder [10]. In-plane substitutions introduce strong disorder effects, which is far less understood [11]. In particular, there is very little information about how magnetic dynamics change, for example, close to the geometrical percolation threshold ∼40% above which magnetic patches are disconnected [3].

The layered iridate Sr_2IrO_4 has recently emerged as a novel antiferromagnetic insulator with close structural and electronic analogies to the cuprates [12–15]. Furthermore, single crystals of $Sr_2Ir_{1-x}M_xO_4$ can be produced where Ir is substituted with a different transition metal M over a wide range [16–20]. This, combined with recent progress in applying resonant inelastic x-ray scattering (RIXS) [9,21] to iridates [22–26], provides an excellent opportunity to determine the magnetic interactions and correlations in disordered (pseudo)spin-1/2 Heisenberg antiferromagnets.

In this paper, we investigate the evolution of magnetic excitations in the heavily disordered regime of $Sr_2Ir_{1-x}Ru_xO_4$. The magnetic correlations survive at least to a high Ru doping of $x = 0.77$. A magnetic gap develops as early as $x = 0.27$ and increases with higher Ru dopings from around 40 meV to 150 meV. Eventually the magnetic excitations become localized and nondispersive throughout the Brillouin zone. With the aid of density-functional theory, we clarify the local electronic structure and the magnetic coupling in the disordered Ir-O-Ru plane. The giant gap originates from a novel easy-axis anisotropic exchange interaction between Ir $J_{\text{eff}} = 1/2$ and Ru $s = 1$ moments. A quantitative description of the localized antiferromagnetic excitations is presented within coherent potential approximation (CPA).

Single crystals of $Sr_2Ir_{1-x}Ru_xO_4$ were grown from off-stoichiometric quantities of $SrCl_2$, $SrCO_3$, IrO_2, and RuO_2 using self-flux techniques [18]. Figure 1(a) shows the magnetic behavior of $Sr_2Ir_{1-x}Ru_xO_4$ which undergoes a crossover from antiferromagnetic (AFM) to paramagnetic (PM) around $x \sim 0.50$. Further information on sample growth and characterizations are provided in Ref. [18] and the Supplemental Material [27].

The RIXS measurements were performed at the Ir L_3 edge using the MERIX endstation (27-ID-B) at the Advanced Photon Source, Argonne National Laboratory, with a total energy resolution of 80 meV (full width at half maximum) and momentum resolution of 0.23 Å^{-1}. All data presented were taken at the base temperature of the cryostat ∼12 K. Figure 1(b) plots RIXS spectra of $Sr_2Ir_{1-x}Ru_xO_4$ over a wide energy window up to 5 eV. There are three distinctive energy-loss features, around 200 meV, 700 meV, and 3.5 eV, respectively. The latter two peaks are orbital excitations of the hole in the valence band, providing information on the electronic

_____
*ycao@bnl.gov
†xliu@aphy.iphy.ac.cn
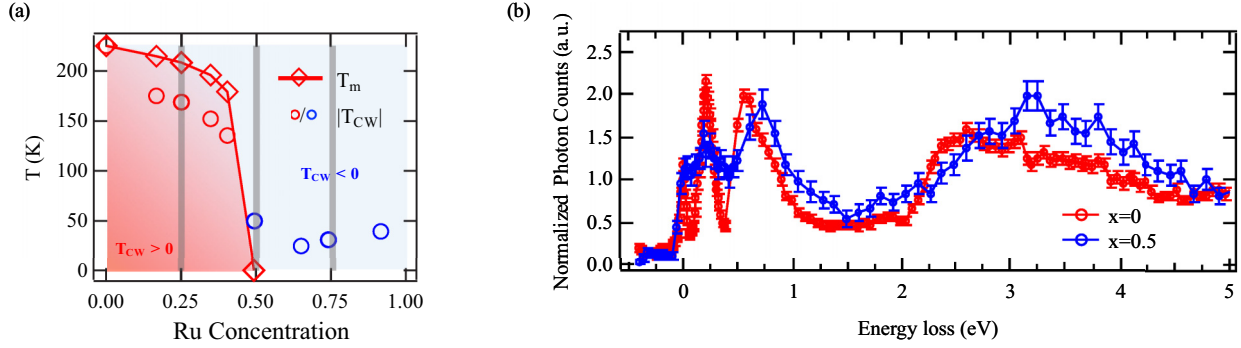‡wenhuxu@bnl.gov
§mdean@bnl.gov

FIG. 1. (a) The magnetic phase diagram of $Sr_2Ir_{1-x}Ru_xO_4$. T_m is the onset temperature for an increased magnetization under an external field of 0.1 T. Around $x = 0.50$, T_m is suppressed to zero. This is also where the Curie-Weiss temperature, T_{C-W}, changes sign [18]. Gray bars mark the select Ru concentrations studied in this work. (b) RIXS spectra of Sr_2IrO_4 and $Sr_2Ir_{0.5}Ru_{0.5}O_4$ at $(\pi,0)$ over a 5.5 eV window, showing persistent excitations centered around 200 meV, 700 meV, and 3.5 eV. These are assigned to magnetic, intra-t_{2g}, and $t_{2g} \rightarrow e_g$ processes, respectively.

configuration of the doped and parent compounds. Specifically, the 3.5 eV peak corresponds to the $t_{2g} \rightarrow e_g$ excitation. Its increase in energy with Ru concentration is consistent with what is expected due to structural changes. Going from $x = 0$ to $x = 0.50$ doping, the Ir-O octahedra elongate by 1.0% along the apex, and contract by 2.9% in-plane [18], increasing the crystal field splitting and moving the $t_{2g} \rightarrow e_g$ feature to higher energies. By comparing to Sr_2IrO_4, we assign the energy-loss peak around 700 meV to the intra-t_{2g} transition, or more precisely, the transition between the Ir 5d $J_{eff} = 1/2$ and $J_{eff} = 3/2$ states [22,23]. By the same token, we deem the energy-loss peak around 200 meV as magnetic in nature, arising from the pseudospin flip.

With increasing Ru concentration all three peaks persist with comparable energy scales. Thus the Ir electronic configuration does not change dramatically, and the $J_{eff} = 1/2$ and $J_{eff} = 3/2$ states are still present at these higher Ru concentrations. In Sr_2IrO_4 and Sr_2RuO_4, Ir^{4+} and Ru^{4+} have formal electron configurations of $5d^5$ and $4d^4$, respectively. As dc resistivity reduces with Ru concentration [18], one might naïvely assume that the numbers of d electrons on Ru and Ir get closer to an average of 4.5, due to increased electron itinerancy. This would indicate effective hole doping on the Ir site into the $J_{eff} = 1/2$ level, with drastic changes in the local electronic structure. In contrast, our data seem to suggest that Ir maintains a formal valence of 4^+, which we will now examine using first-principles calculations.

We calculate the orbital configuration of $Sr_2Ir_{1-x}Ru_xO_4$ in the GGA+U implementation of the density functional theory [27]. Table I lists the calculated electron occupation number on the Ir and Ru d orbitals vs Ru concentration. Up to $x > 0.75$ the numbers of d electrons on Ir/Ru have relatively small changes compared to the doped Ru concentration, especially when a spin-polarized ground state is considered. Thus both Ir/Ru sites maintain a valence close to 4^+, similar to those in Sr_2IrO_4/Sr_2RuO_4, in agreement with the x-ray absorption experiments in Ref. [19]. We project the d electron density of states onto the Ir/Ru orbitals and find that the $J_{eff} = 1/2$ and $J_{eff} = 3/2$ are indeed robust. This is because for each individual Ir-O octahedron, the spin-orbit coupling energy scale [12,28] ($\sim$400 meV) dominates over the tetragonal

splitting between t_{2g} levels, giving rise to a relatively well-defined pseudospin-1/2 state [28,29]. This interpretation also agrees with the persistence of the insulating phase up to $x \simeq 0.50$ in $Sr_2Ir_{1-x}Ru_xO_4$ [18]. In our calculation, the electrons near the Fermi level come primarily from the local Ru-O octahedra and cannot move freely especially for low Ru concentrations. GGA+U calculations for all Ru concentrations favor spin-polarized ground states, with antiferromagnetic couplings between the nearest-neighbor Ir $J_{eff} = 1/2$ and Ru $s = 1$ (pseudo)spins. We therefore consider that the effect of Ru doping in $Sr_2Ir_{1-x}Ru_xO_4$ is primarily to introduce substitutional $s = 1$ magnetic disorder (rather than charge doping) for a large range of Ru concentration (until the material gets sufficiently close to Sr_2RuO_4). We show later that phenomenological CPA simulations, based on this picture, account for the observed magnetic dispersion.

In Figs. 2(a)–2(c) we take a closer look at the excitations within the first 1.5 eV of energy loss as $Sr_2Ir_{1-x}Ru_xO_4$ crosses the AFM-PM phase boundary: (a) $x = 0.27$, (b) $x = 0.50$, and (c) $x = 0.77$. All dopings are marked with gray bars in the phase diagram in Fig. 1(a). We assign the $(\pi,0)$ direction to be parallel to the nearest neighbor Ir-Ir bond directions, in analogy with the usual definition in square-net cuprates. As expected in a disordered system, both the magnetic and orbital excitations are broader than in the undoped Sr_2IrO_4. We fit the elastic peak and the two excitations with three Gaussian peaks on top of a smooth background, and the fitted energies of the magnetic and orbital modes are shown in Fig. 2(d).

TABLE I. The number of d electrons on each Ir/Ru site, derived from GGA+U calculations. We used $U = 2$ eV [12] for Ir and $U = 3$ eV for Ru. NM and SP stand for the nonmagnetic and spin-polarized calculations, respectively.

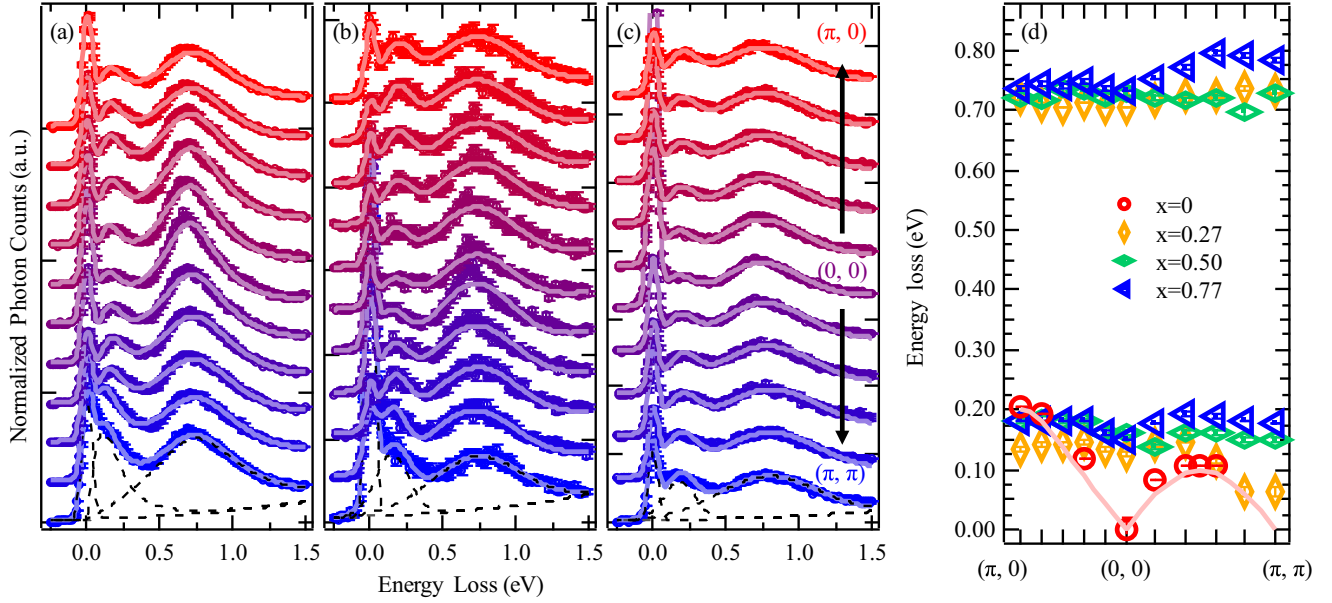| Ru concentration		0%	25%	50%	100%
Ir	NM	5.20	5.16	5.19	
	SP	5.20	5.19	5.21	
Ru	NM		4.53	4.61	4.47
	SP		4.58	4.47	4.46

FIG. 2. (a)–(c) The energy-loss spectra along $(\pi,0)$-$(0,0)$-(π,π) high symmetry directions for three Ru dopings (a) $x = 0.27$, (b) $x = 0.50$, and (c) $x = 0.77$. The solid thick lines are fits to the RIXS data. The dashed black curves are the individual components of the fit for the energy loss curve at (π,π). (d) Energies of the magnetic and orbital excitations as a function of momentum transfer for different Ru concentrations. Error bars represent the uncertainty from the least-mean square fitting algorithm. The pink solid line is the fitted magnon dispersion in Sr_2IrO_4 reproduced from Ref. [22].

The most striking feature is that the antiferromagnetic excitations persist up to at least $x = 0.77$ and that the maximum energy scale of the magnetic excitations at high dopings is comparable to that in undoped Sr_2IrO_4. In a simple mean-field description, the overall magnetic excitation energy would be expected to decrease appreciably due to lower magnon energies in Sr_2RuO_4. The results here reflect the strong local correlation in the material that voids mean-field descriptions. Such a result is reminiscent of studies of electron and hole doped cuprates and iridates [6–9,24,25,30–32], albeit up to smaller maximum doping level of 40% in cuprates and a mere 10% in iridates. Specifically, the magnetic excitation energies at $(\pi,0)$ are robust against doped charge carriers and in this work disorder, while profound changes take place around, e.g., (π, π) and $(\pi/2, \pi/2)$ [7,8,24,25,33]. This similarity is not necessarily expected as it involves comparing the effects of itinerant carriers introduced by out-of-plane atomic substitutions with in-plane replacement of the Ir atoms.

The second observation is that a large spin gap already opens for $x = 0.27$ and appears to increase and saturate with Ru doping across the phase transition. This is in sharp contrast to the dispersive, almost gapless paramagnetic excitations in the electron and hole doped cuprates and iridates mentioned above. At higher doping of $x = 0.50$ and $x = 0.77$, the magnetic gaps are larger than 150 meV and severely dampened. Such an energy scale lies between the zone boundary energy scales of Sr_2IrO_4: $\sim$200 meV at $(\pi,0)$ and $\sim$100 meV at $(\pi/2,\pi/2)$.

The opening up of a finite gap in the spin excitation spectrum can be explained by broken continuous rotational symmetry. In our case, a plausible origin of spin gap is the anisotropic antiferromagnetic exchange between t_{2g} electrons experiencing different spin-orbit coupling on the Ru $4d$ and

Ir $5d$ orbitals [34], as well as the strong Hund's coupling on the Ru $4d$ orbitals. We illustrate this by considering the toy model in Fig. 3. For a pair of Ru-Ir spins, after projecting out the oxygen states, the effective magnetic Hamiltonian $\mathcal{H} = \mathcal{H}_{SO} + \mathcal{H}_{Hund} + \mathcal{H}_{AF}$ consists of the spin-orbit coupling $\mathcal{H}_{SO}$ on the Ir sites, the Hund's coupling $\mathcal{H}_{Hund}$ between the t_{2g} spins on the Ru site, and the antiferromagnetic coupling between Ru and Ir spins, $\mathcal{H}_{AF} = J_{yz}\mathbf{s}_{Ru,yz} \cdot \mathbf{s}_{Ir1,yz} + J_{xy}\mathbf{s}_{Ru,xy} \cdot \mathbf{s}_{Ir1,xy} + J_{zx}\mathbf{s}_{Ru,zx} \cdot \mathbf{s}_{Ir2,zx} + J_{xy}\mathbf{s}_{Ru,xy} \cdot \mathbf{s}_{Ir2,xy}$. As a first-order perturbation to $\mathcal{H}_{SO}$, $\mathcal{H}_{AF}$ induces an effective anisotropic coupling between the t_{2g} spins on Ru and the pseudospin (instead of physical spin) $\mathbf{J}_{eff}$ on Ir [34].
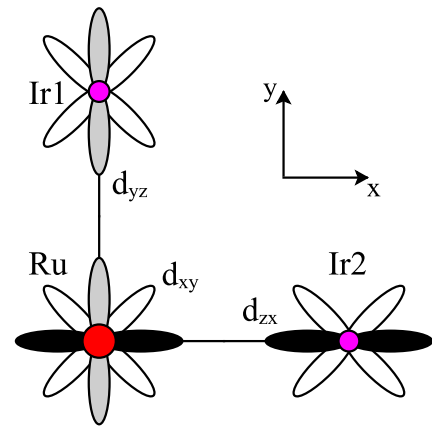

FIG. 3. Geometry of Ru-Ir bonds with orbitals active t_{2g} orbitals along these bonds (top view). Black: d_{zx} orbitals. Gray: d_{yz} orbitals. White: d_{xy} orbitals. The oxygen atoms between the nearest-neighbor Ir atoms are not displayed, and the oxygen states have been projected out in the effective superexchange model.
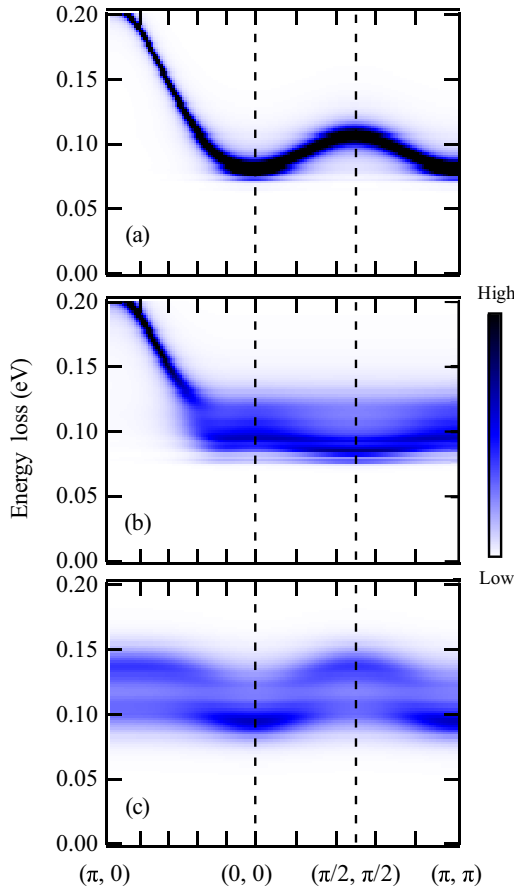
FIG. 4. (a) and (b) Magnetic excitations calculated using CPA with (a) $x = 0.25$ and (b) $x = 0.50$ concentrations of $s = 1$ moments (to simulate the Ru sites), preserving both the nearest neighbor (NN) and next-nearest-neighbor (NNN) magnetic interactions between $J_{\text{eff}} = 1/2$ sites. (c) Calculated magnetic excitations with 50% $s = 1$ moments. The couplings between the NNN and further $J_{\text{eff}} = 1/2$ moments are suppressed.

For example, the effective coupling on the Ru-Ir2 bond, $\mathcal{H}_{\text{AF2}} = J_{zx}/3(s^x_{\text{Ru},zx} J^x_{\text{Ir2, eff}} - s^y_{\text{Ru},zx} J^y_{\text{Ir2, eff}} + s^z_{\text{Ru},zx} J^z_{\text{Ir2, eff}}) + J_{xy}/3(s^x_{\text{Ru},xy} J^x_{\text{Ir2, eff}} + s^y_{\text{Ru},xy} J^y_{\text{Ir2, eff}} + s^z_{\text{Ru},xy} J^z_{\text{Ir2, eff}})$, has an easy z-x plane. Similarly, the effective coupling on the Ru-Ir1 bond has an easy y-z plane. The Hund's coupling on the Ru site, $\mathcal{H}_{\text{Hund}} = -J_H \mathbf{S}^2_{\text{Ru}}$, where $\mathbf{S}_{\text{Ru}} = \mathbf{s}_{\text{Ru},xy} + \mathbf{s}_{\text{Ru},yz} + \mathbf{s}_{\text{Ru},xz}$ favors aligning the Ru t_{2g} spins. If one Ru site is connected to neighboring Ir sites by at least two perpendicular Ru-Ir bonds (as in Fig. 3), the degeneracy of rotating $\mathbf{s}_{\text{Ru},yz}$ in the y-z plane and $\mathbf{s}_{\text{Ru},zx}$ in the z-x plane will be lifted by $\mathcal{H}_{\text{Hund}}$, giving rise to the effective anisotropic exchange with an easy z axis.

We capture the geometrical impact of introducing spin disorder and spin anisotropy on the system using the coherent potential approximation (CPA) [35,36] following the recipe in Ref. [36] and calculate the magnetic excitation spectrum

(Fig. 4) [37]. The nearest neighbor (NN) coupling between Ir sites is selected to be $J_{\text{Ir-Ir}} = 60$ meV, identical to that in Sr$_2$IrO$_4$. We extract nearest-neighbor Ir-Ru coupling $J_{\text{Ir-Ru}} \simeq 60$ meV from the energy differences between the magnetic and paramagnetic ground states calculated using GGA+U. Other input exchange energies for the CPA calculation includes the exchange between next- (NNN) and next-next-nearest (NNNN) neighboring $J_{\text{eff}} = 1/2$ pseudospins, $J'_{\text{Ir-Ir}} = -20$ meV, and $J''_{\text{Ir-Ir}} = 15$ meV, respectively [22,23]. As to the exchange between NN $s = 1$ spins, there is no qualitative change in the simulated magnetic excitation for a weak antiferromagnetic $J_{\text{Ru-Ru}} \lesssim 5$ meV. Figures 4(a) and 4(b) show increased magnetic gaps at $(0,0)$ and (π,π) with rising $s = 1$ concentrations. At $x = 0.50$ in Fig. 4(b), the magnetic excitations are damped and flattened around much of the Brillouin zone, except along $(\pi,0)$—$(0,0)$ where the excitation spectrum is barely affected by the disorder. To further increase the simulated magnetic gap, we set $J'_{\text{Ir-Ir}}$ and $J''_{\text{Ir-Ir}}$ to zero, and the calculations are shown in Fig. 4(c). The magnetic excitation is turned into a heavily damped localized mode, recapturing the dispersionless feature in Fig. 2(d). The suppression of the NNN and NNNN exchange energies may reflect that the corresponding magnetic couplings are destroyed geometrically in the presence of more $s = 1$ disorders.

In summary, we have measured the magnetic excitations in Sr$_2$Ir$_{1-x}$Ru$_x$O$_4$ across a wide doping range and observed a crossover from dispersive to gapped, localized magnons. First-principles calculations and simulations using the coherent potential approximations provide a thorough description of these findings based on disorder and local anisotropy effects. Similar effects are likely to be at play in other heavily doped transition metal oxides, with important implications for understanding the importance of disorder on magnetic correlations, which is a vital prerequisite for modeling their emergent phenomena.

[1] S. Sachdev, C. Buragohain, and M. Vojta, Science **286**, 2479 (1999).

[2] P. A. Lee, N. Nagaosa, and X.-G. Wen, Rev. Mod. Phys. **78**, 17 (2006).

[3] O. P. Vajk, P. K. Mang, M. Greven, P. M. Gehring, and J. W. Lynn, Science **295**, 1691 (2002).

[4] D. J. Scalapino, Rev. Mod. Phys. **84**, 1383 (2012).

[5] C. J. Jia, E. A. Nowadnick, K. Wohlfeld, Y. F. Kung, C.-C. Chen, S. Johnston, T. Tohyama, B. Moritz, and T. P. Devereaux, Nat. Commun. **5**, 3314 (2014).

[6] M. P. M. Dean, G. Dellea, R. S. Springell, F. Yakhou-Harris, K. Kummer, N. B. Brookes, X. Liu, Y. J. Sun, J. Strle, T. Schmitt *et al.*, Nat. Mater. **12**, 1019 (2013).

[7] K. Ishii, M. Fujita, T. Sasaki, M. Minola, G. Dellea, C. Mazzoli, K. Kummer, G. Ghiringhelli, L. Braicovich, T. Tohyama, K. Tsutsumi, K. Sato, R. Kajimoto, K. Ikeuchi, K. Yamada, M. Yoshida, M. Kurooka, and J. Mizuki, Nat. Commun. **5**, 3714 (2014).

[8] W. S. Lee, J. J. Lee, E. A. Nowadnick, S. Gerber, W. Tabis, S. W. Huang, V. N. Strocov, E. M. Motoyama, G. Yu, B. Moritz *et al.*, Nat. Phys. **10**, 883 (2014).

[9] M. P. M. Dean, J. Magn. Magn. Mater. **376**, 3 (2015).

[10] H. Alloul, J. Bobroff, M. Gabay, and P. J. Hirschfeld, Rev. Mod. Phys. **81**, 45 (2009).

[11] Calculations on spin excitations and long-range order in diluted quantum antiferromagnets were presented in, e.g., A. L. Chernyshev, Y.-C. Chen, and A. H. Castro Neto, Phys. Rev. Lett. **87**, 067209 (2001); Phys. Rev. B **65**, 104407 (2002).

[12] B. J. Kim, H. Jin, S. J. Moon, J.-Y. Kim, B.-G. Park, C. S. Leem, J. Yu, T. W. Noh, C. Kim, S.-J. Oh *et al.*, Phys. Rev. Lett. **101**, 076402 (2008).

[13] B. J. Kim, H. Ohsumi, T. Komesu, S. Sakai, T. Morita, H. Takagi, and T. Arima, Science **323**, 1329 (2009).

[14] Y. K. Kim, O. Krupin, J. D. Denlinger, A. Bostwick, E. Rotenberg, Q. Zhao, J. F. Mitchell, J. W. Allen, and B. J. Kim, Science **345**, 187 (2014).

[15] Y. Cao, Q. Wang, J. A. Waugh, T. J. Reber, H. Li, X. Zhou, S. Parham, S.-R. Park, N. C. Plumb, E. Rotenberg, A. Bostwick *et al.*, Nat. Commun. **7**, 11367 (2016).

[16] J. P. Clancy, A. Lupascu, H. Gretarsson, Z. Islam, Y. F. Hu, D. Casa, C. S. Nelson, S. C. LaMarra, G. Cao, and Young-June Kim, Phys. Rev. B **89**, 054409 (2014).

[17] F. Ye, X. Wang, C. Hoffmann, J. Wang, S. Chi, M. Matsuda, B. C. Chakoumakos, J. A. Fernandez-Baca, and G. Cao, Phys. Rev. B **92**, 201112 (2015).

[18] S. J. Yuan, S. Aswartham, J. Terzic, H. Zheng, H. D. Zhao, P. Schlottmann, and G. Cao, Phys. Rev. B **92**, 245103 (2015).

[19] S. Calder, J. W. Kim, G.-X. Cao, C. Cantoni, A. F. May, H. B. Cao, A. A. Aczel, M. Matsuda, Y. Choi, D. Haskel, B. C. Sales, D. Mandrus, M. D. Lumsden, and A. D. Christianson, Phys. Rev. B **92**, 165128 (2015).

[20] A. Glamazda, W.-J. Lee, K.-Y. Choi, P. Lemmens, H. Y. Choi, N. Lee, and Y. J. Choi, Phys. Rev. B **89**, 104406 (2014).

[21] L. J. P. Ament, M. van Veenendaal, T. P. Devereaux, J. P. Hill, and J. van den Brink, Rev. Mod. Phys. **83**, 705 (2011).

[22] J. Kim, D. Casa, M. H. Upton, T. Gog, Y.-J. Kim, J. F. Mitchell, M. Van Veenendaal, M. Daghofer, J. van den Brink, G. Khaliullin *et al.*, Phys. Rev. Lett. **108**, 177003 (2012).

[23] J. Kim, M. Daghofer, A. H. Said, T. Gog, J. van den Brink, G. Khaliullin, and B. J. Kim, Nat. Commun. **5**, 4453 (2014).

[24] X. Liu, M. P. M. Dean, Z. Y. Meng, M. H. Upton, T. Qi, T. Gog, Y. Cao, J. Q. Lin, D. Meyers, H. Ding *et al.*, Phys. Rev. B **93**, 241102 (2016).

[25] H. Gretarsson, N. H. Sung, J. Porras, J. Bertinshaw, C. Dietl, Jan A. N. Bruin, A. F. Bangura, Y. K. Kim, R. Dinnebier, Jungho Kim, A. Al-Zein, M. Moretti Sala, M. Krisch, M. Le Tacon, B. Keimer, and B. J. Kim, Phys. Rev. Lett. **117**, 107001 (2016).

[26] M. P. M. Dean, Y. Cao, X. Liu, S. Wall, D. Zhu, R. Mankowsky, V. Thampy, X. M. Chen, J. G. Vale, D. Casa *et al.*, Nat. Mater. **15**, 601 (2016).

[27] See Supplemental Material at http://link.aps.org/supplemental/10.1103/PhysRevB.95.121103 for further details of the sample growth, sample characterization and density functional calculations.

[28] X. Liu, V. M. Katukuri, L. Hozoi, W.-G. Yin, M. P. M. Dean, M. H. Upton, J. Kim, D. Casa, A. Said, T. Gog *et al.*, Phys. Rev. Lett. **109**, 157401 (2012).

[29] G. Jackeli and G. Khaliullin, Phys. Rev. Lett. **102**, 017205 (2009).

[30] B. Vignolle, S. M. Hayden, D. F. McMorrow, H. M. Rønnow, B. Lake, C. D. Frost, and T. G. Perring, Nat. Phys. **3**, 163 (2007).

[31] O. J. Lipscombe, S. M. Hayden, B. Vignolle, D. F. McMorrow, and T. G. Perring, Phys. Rev. Lett. **99**, 067002 (2007).

[32] M. P. M. Dean, R. S. Springell, C. Monney, K. J. Zhou, J. Pereiro, I. Božović, B. Dalla Piazza, H. M. Rønnow, E. Morenzoni, J. van den Brink *et al.*, Nat. Mater. **11**, 850 (2012).

[33] M. Fujita, H. Hiraka, M. Matsuda, M. Matsuura, J. M. Tranquada, S. Wakimoto, G. Xu, and K. Yamada, J. Phys. Soc. Jpn. **81**, 011007 (2011).

[34] W.-G. Yin, X. Liu, A. M. Tsvelik, M. P. M. Dean, M. H. Upton, J. Kim, D. Casa, A. Said, T. Gog, T. F. Qi, G. Cao, and J. P. Hill, Phys. Rev. Lett. **111**, 057202 (2013).

[35] W. J. L. Buyers, T. M. Holden, E. C. Svensson, R. A. Cowley, and R. W. H. Stevenson, Phys. Rev. Lett. **27**, 1442 (1971).

[36] W. J. L. Buyers, D. E. Pepper, and R. J. Elliott, J. Phys. C **5**, 2611 (1972).

[37] Sophisticated direct simulations of disorder with many large supercells will be published elsewhere.